frontiers | Frontiers in Earth Science

TYPE Original Research
PUBLISHED 11 November 2022
DOI 10.3389/feart.2022.841483

OPEN ACCESS

EDITED BY
Andrew James Manning,
HR Wallingford, United Kingdom

REVIEWED BY
Kyungsik Choi,
Seoul National University, South Korea
Tomas Fernández-Montblanc,
University of Cádiz, Spain

*CORRESPONDENCE
Zhenchang Zhu,
zhenchang.zhu@gdut.edu.cn

SPECIALTY SECTION
This article was submitted to Marine Geoscience,
a section of the journal
Frontiers in Earth Science

RECEIVED 22 December 2021
ACCEPTED 31 October 2022
PUBLISHED 11 November 2022

CITATION
Zhu Q, Nie W, Zhu Z, Cai Y and Yang Z (2022), Sensitivity of sheltered mudflats to wind events.
Front. Earth Sci. 10:841483.
doi: 10.3389/feart.2022.841483

Sensitivity of sheltered mudflats to wind events

Qin Zhu[1], Wei Nie[2], Zhenchang Zhu[1,2]*, Yanpeng Cai[1,2] and Zhifeng Yang[1,2]

[1]Southern Marine Science and Engineering Guangdong Laboratory (Guangzhou), Guangzhou, China, [2]Guangdong Provincial Key Laboratory of Water Quality Improvement and Ecological Restoration for Watersheds, Institute of Environmental and Ecological Engineering, Guangdong University of Technology, Guangzhou, China

The impact of waves on the morphological changes of sheltered mudflats is less well studied compared to that on open flats. To investigate the sensitivity of low-energy sheltered mudflats to hydrodynamics such as waves, we carried out *in situ* measurements of bed level, currents, and waves on the middle flat of a sheltered mudflat in a bay in southern China. Two 1-month measurements, March 26–26 April 2021, and July 8–8 August 2021, were performed for repetition. We found that the sheltered system was not as stable as it appeared. The maximum intratidal bed-level variation, ΔZ, was <5 mm in calm conditions. However, wind speeds slightly highly than 3.0 m/s, under which significant wave height was approximately 0.1 m, triggered significant bed-level variation patterns, with ΔZ reaching up to 2 cm. Intratidal bed-level change patterns depend on the relative dominance of waves and currents: low τ_c (current-induced bed shear stress) and high τ_w (wave-induced bed shear stress) promote the generation and migration of bed ripples; comparable τ_c and τ_w, with medium-to-high values, lead to non-cyclic bed-level change patterns; high τ_c and high τ_w result in bed accumulation/degradation superimposed by bed ripple migration. From a long-term perspective, i.e. in the time scale of month to year, sheltered mudflats are stable systems, and their high sensitivity causes short-term significant bed-level variation. The sensitivity and stability of sheltered mudflats must be further investigated to explore the effects of human intervention and global climate change.

KEYWORDS

sheltered mudflat, bed level change, bed sensitivity, wind event, intratidal highresolution measurements

Introduction

The morphodynamics of tidal mudflats have been extensively studied in recent decades as they serve vital ecological and environmental functions in addition to protecting shorelines (Costanza et al., 1997; Friedrichs, 2011; Goodwin et al., 2016). Among various tidal flats, tidal flats in sheltered settings, such as lagoons, back-barrier flats, flats in bays, and fringing flats in estuaries, are important as they form relatively stable environments that maintain biodiversity and healthy marine ecosystems (Chakraborty, 2001; Callaghan et al., 2010; Waska and Kim, 2010; Paavo et al., 2012;

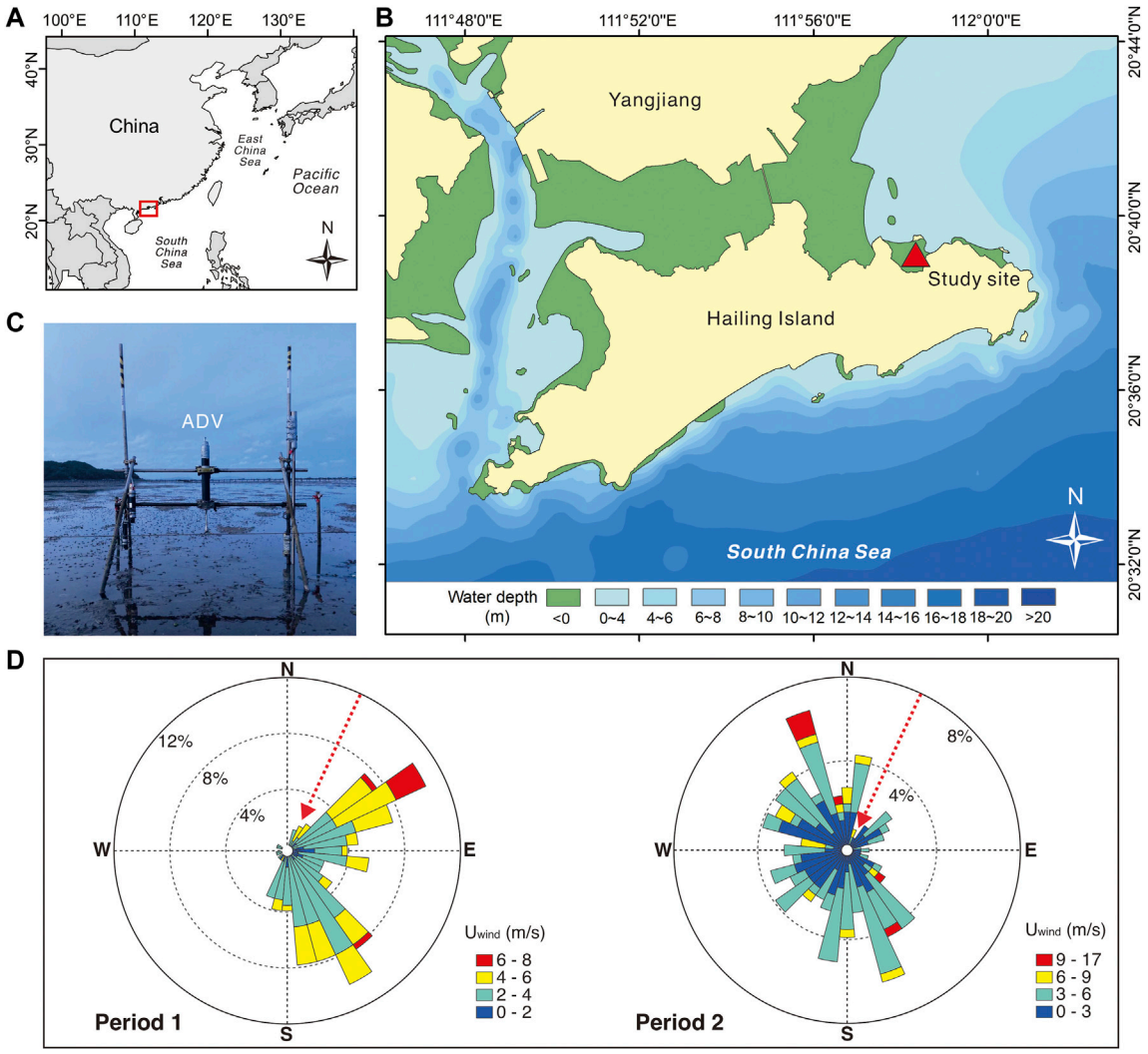

FIGURE 1
(A) Location of the study site near the west Pacific Ocean. **(B)** Map of Hailing Island with the observation site and wind gauge. **(C)** Photograph of the deployed instrument. **(D)** Wind roses of Period 1 (March 26–26 April 2021) and Period 2 (July 8–8 August 2021). The red arrow indicates the orientation of the bay.

Reckhardt et al., 2015). These sheltered flats are generally mud dominated owing to the low-energy setting (Madsen et al., 2010; McLachlan et al., 2020).

Compared to sheltered mudflats, the morphodynamics of open flats, which are exposed to stronger hydrodynamics, have received more attention as they are believed to be more strongly impacted by tropical cyclones and hurricanes (Li et al., 2000; Yang et al., 2005; Fan et al., 2006; MacMahan et al., 2010; Zhu et al., 2016). Although sheltered mudflats are protected from the more energetic ocean waves, they are still influenced by diffracted waves and local wind waves (Klein and de Menezes, 2001; Ryu, 2003; Shen et al., 2018; Siegle et al., 2018). Bed shear stress, which is a critical parameter in sediment dynamics on tidal flats, results from the nonlinear interaction between currents and waves (Grant and Madsen, 1979; van Rijn, 1993). The role of waves has been frequently discussed in the situation of open flats, while has been underestimated for sheltered flats. Natural hydrodynamic condition, together with human activities, can alter the depositional environment at different temporal and spatial scales (Blum and Roberts, 2009; Yang et al., 2011; Wang et al., 2015). The study of hydrodynamics and bed stability of sheltered mudflats is also essential to local ecosystems and environments, as sheltered habitats with high productivity are more sensitive to contaminants (Nansingh and Jurawan, 1999; Reckhardt et al., 2015). Therefore, it is important to develop an understanding of how sheltered mudflats react to dynamic processes, especially waves, in the context of increasing threats from anthropogenic disturbances and global climate change

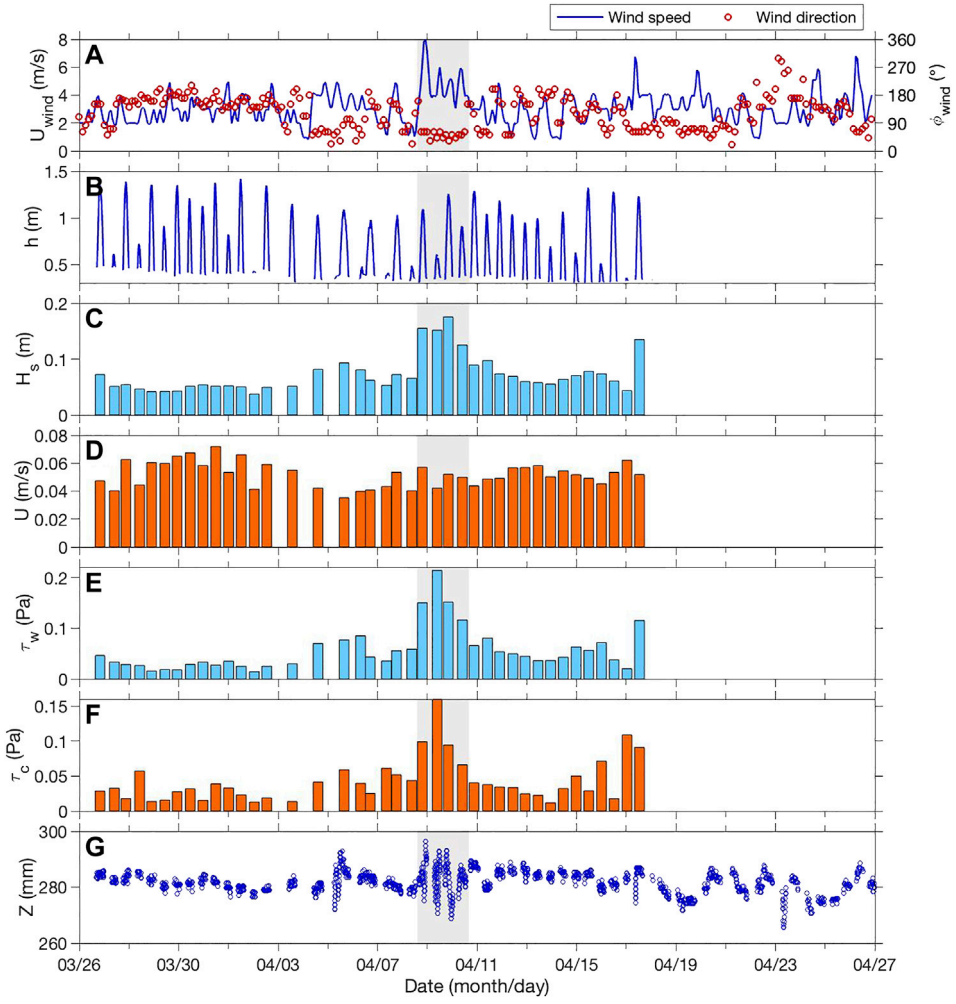

FIGURE 2
Time series of **(A)** wind speed (U_{wind}), **(B)** water depth (h), **(C)** significant wave height (H_s), **(D)** horizontal current velocity (U), **(E)** wave-induced bed shear stress (τ_w), **(F)** current-induced bed shear stress (τ_c), and **(G)** relative bed level (Z) change during Period 1.

(Nicholls et al., 1999; Walling, 2006; Vafeidis et al., 2008; Milliman and Farnsworth, 2011; Temmerman et al., 2013; Schuerch et al., 2018; Liu et al., 2020).

Intratidal measurements elucidate the details of bed-level changes that, in combination with wave and current action data, are key to understanding the mechanisms of bed erosion and deposition (Andersen et al., 2006; Zhu et al., 2014). In particular, for a low-energy dynamic system with slight bed-level changes, bed-level data from daily to monthly morphological surveys (Bassoullet et al., 2000; Fan et al., 2006) may not suffice. Measurements of intratidal bed-level changes have been restricted until the recent development of acoustic ranging measurements, such as ALTUS, altimeter, and extra ADV beams (Gallagher et al., 1996; Jestin et al., 1998; Thornton et al., 1998; Christie et al., 1999; Saulter et al., 2003; Andersen et al., 2007; Turner et al., 2008; Zhu et al., 2017). To date, acoustic ranging measurement is the only approach for obtaining bed-level data during submergence in high temporal (interval in minutes) and spatial (accuracy of ± 1–2 mm) resolution.

In this study, we deployed an acoustic Doppler velocimeter (ADV) to obtain data on bed-level changes, as well as currents and wave parameters, on a sheltered mudflat. Our objective was to investigate whether sheltered mudflats are as stable as they appear by: 1) elucidating the response of bed-level changes in sheltered mudflats to variables of environmental forces, such as wind, waves, and currents; and 2) examine the morphological sensitivity of sheltered mudflat beds to hydrodynamics, especially waves. This work is intended to deepen our understanding of the bed stability of sheltered mudflats under different pressure scenarios.

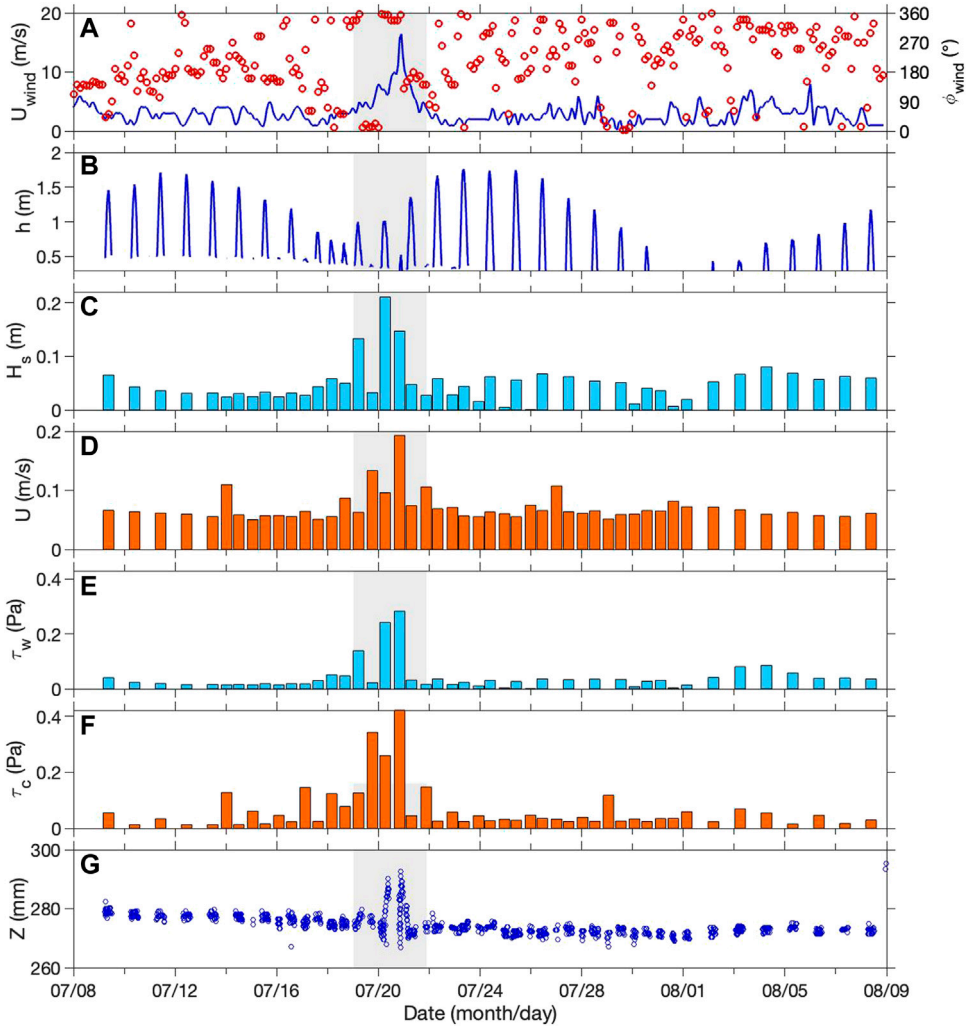

FIGURE 3
Time series of **(A)** wind speed (U_{wind}), **(B)** water depth (h), **(C)** significant wave height (H_s), **(D)** horizontal current velocity (U), **(E)** wave-induced bed shear stress (τ_w), **(F)** current-induced bed shear stress (τ_c), and **(G)** relative bed level (Z) change during Period 2.

Material and methods

Study site

In situ observations were conducted on a sheltered mudflat of Hailing Island, which is located on the west bank of the Pearl River Estuary, China (Figure 1A). According to records from the tide gauge on the west side of the island, the local tides are mixed semi-diurnal with an average of 2.5 m in tidal range. The spring and neap tidal ranges are >3.0 m and 0.5 m, respectively. Monsoon-driven winds are predominantly north-easterly in autumn and winter, south-easterly in spring, and southerly in summer. The multi-year average wind speed is 4.2 m/s. The province, where the study area is located, is hit by 3.6 tropical cyclones per year on average, which is the highest in China. Waves in this area are dominated by wind waves with a frequency of approximately 85%, and the average wave height is 0.2 m with the maximum storm surge reaching over 2 m.

The study site (111°58′42″E, 21°39′2″N) is located on the middle flat (at the mean water level) of the mangrove wetland on the northeast side of Hailing Island (Figure 1B). The south side of the island is open sea, while the north side is connected with an intertidal area. The tidal flat has a long-shore length of 2.4 km and a cross-shore length of 1.6 km. The mudflat faces to north-east-north (25°), with a mean slope of 2.5‰ (Hu et al., 2020). The upper flat is covered by dense mangrove forest, with a height of 2–3 m. As the study area is located in a bay on the back side of the open sea and a barrier island exists at the seaside of the bay, the

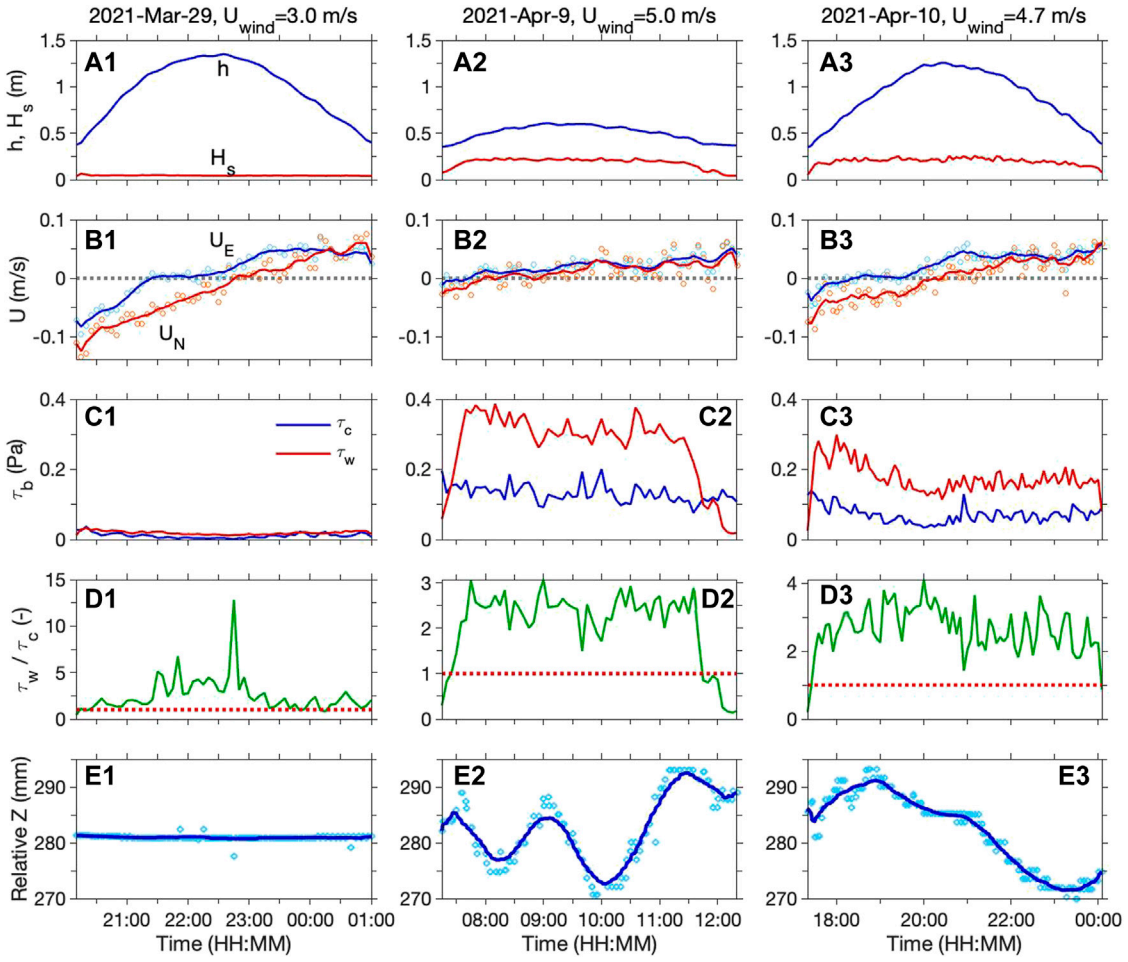

FIGURE 4
Time series of **(A)** water level (h), significant wave height (H_s), **(B)** eastward (U_E) and northward (U_N) current velocities, **(C)** current- and wave-induced bed shear stress (τ_c and τ_w), **(D)** ratio of τ_w and τ_c, and **(E)** relative bed level (Z) changes during Period 1.

study area is relatively sheltered. Therefore, the mangrove wetland provides an ideal habitat for benthos and birds, thereby sustaining high biodiversity in the region (Zhu et al., 2008; Hu et al., 2020).

Instrumentation setup

An ADV (6.0 MHz vector current meter, Nortek AS, Norway) attached to an H-shaped sedimentary measurement frame was used to measure the three-dimensional flow velocities at a high sampling rate (Figure 1C) from March 26 to 26 April 2021 (Period 1), and from July 8 to 8 August 2021 (Period 2). The ADV recorded velocities and pressure with a burst interval of 5 min for a period of 300 s at a frequency of 16 Hz. The water pressure, measured by a silicone piezoresistive pressure sensor (Nortek, 2005), was used to analyze wave characteristics (Zhu et al., 2016). Based on the records of the distance between the transmitter of the ADV and the bed sediment surface from the extra acoustic beams of each burst, relative bed levels at high temporal resolution were also measured using ultrasonic echo-ranging with an accuracy of 1 mm (Andersen et al., 2007; Zhu et al., 2017). The accuracy is determined by the sound speed, which is affected by water temperature and salinity, as well as the boundary condition. The acoustic sensor and the pressure sensor were 0.3 m and 0.54 m above the sediment surface, respectively.

Measured wind data of the nearest site (111°58′12″E, 21°52′12″N) was downloaded from Institute for the Environment, the Hong Kong University of Science and Technology (http://envf.ust.hk). The interval of wind speed and wind direction is 3 h.

TABLE 1 Statistics of key hydrodynamic parameters.

		Period 1			Period 2		
		All	Calm	Windy	All	Calm	Windy
Significant wave height, H_s (m)	Mean	0.08	0.06	0.16	0.06	0.04	0.10
	Min	0.03	0.03	0.04	0	0	0.0006
	Max	0.27	0.16	0.27	0.36	0.16	0.36
	Std	0.05	0.02	0.06	0.05	0.03	0.09
Flow velocity, U (m/s)	Mean	0.05	0.05	0.05	0.07	0.06	0.08
	Min	0.0003	0.01	0.39	0.002	0.002	0.002
	Max	0.39	0.34	0	0.45	0.45	0.45
	Std	0.03	0.03	0.03	0.06	0.05	0.07
Wave-induced bed shear stress, τ_w (Pa)	Mean	0.06	0.05	0.16	0.05	0.03	0.11
	Min	0.01	0.01	0.02	0	0	0.0004
	Max	0.39	0.18	0.39	0.86	0.14	0.86
	Std	0.06	0.03	0.09	0.08	0.04	0.15
Current-induced bed shear stress, τ_c (Pa)	Mean	0.03	0.03	0.08	0.05	0.03	0.12
	Min	0.0002	0.0003	0.0002	0.0001	0.0001	0.0008
	Max	0.27	0.27	0.25	0.94	0.94	0.92
	Std	0.04	0.03	0.05	0.11	0.07	0.17
Maximum intratidal bed-level variation, $(\Delta Z)_{TCmax}$ (mm)	Mean	6.4	4.7	18.5	4.6	3.6	9.4
	Max	24.5	17.3	24.5	25.8	12.1	25.8
	Min	1.6	1.6	11.8	1.6	1.6	2.1
	Std	5.1	3.1	5.9	4.6	1.8	9.5

Data processes and calculation

Data filtration was conducted prior to further analyses. The burst datasets with backscatter acoustic amplitude less than 100 counts and correlation less than 50% were removed.

The wave-induced bed shear stress, τ_w, was obtained by analyzing the surface-elevation monitoring data. Significant wave height, H_s, and significant wave period, T_s, were derived from high-frequency pressure data *via* linear wave theory (Tucker and Pitt, 2001) (see http://neumeier.perso.ch/matlab/waves for the routines). The near-bed peak orbital excursion ($\hat{A}_\delta$) and peak orbital velocity ($\hat{U}_\delta$) can be expressed as (van Rijn, 1993):

$$\hat{A}_\delta = \frac{H}{2\sinh(kh)} \tag{1}$$

$$\hat{U}_\delta = \omega\hat{A}_\delta = \frac{\pi H}{T\sinh(kh)} \tag{2}$$

where H is the wave height (m), k=(2 π/L) is the wave number (m^{-1}), with wave length L=(g T^2/2 π)tanh (kh). Where h is the water depth (m), ω is the angular velocity (s^{-1}), and T is the wave period (s). In practice, the significant wave height H_S and significant wave period T_S are used for H and T in the formulae. The time-averaged (over half a wave cycle) bed shear stress caused by waves, τw (Pa), can be expressed as (van Rijn, 1993)

$$\tau_w = \frac{1}{4}\rho_w f_w \hat{U}_\delta^2 \tag{3}$$

where ρ_w is the water density (kg/m^3), and fw is the friction coefficient (-), which is determined by the hydraulic regime (van Rijn, 1993):

$$f_w = \begin{cases} 2Re_w^{-0.5} & , \quad Re_w \le 10^5\,(laminar) \\ 0.0521Re_w^{-0.187} & , \quad Re_w > 10^5\,(smooth\,turbulent) \\ 0.237r^{-0.52} & , \quad (rough\,turbulent) \end{cases} \tag{4}$$

where $Re_w = \frac{\hat{U}_\delta \hat{A}_\delta}{V}$ and $r = \frac{\hat{A}_\delta}{K_S}$ are the wave Reynolds number (-) and relative roughness (-), respectively. Parameter ks is the Nikuradse roughness value given as $k_s = 2.5d_{50}$, where d50 is the median grain size of the bed sediment, and ν is the kinematic viscosity of sea water (m^2/s).

Wave-orbital-motion-induced velocities were removed from the total burst velocities by the moving-average method with a 1-s smooth window (Williams et al., 2003). Subsequently, the turbulent kinetic energy method with vertical fluctuations (TKEw) was used to calculate the bottom bed shear stress τ_c (Pa). The formula is as follows (Kim et al., 2000; Zhu et al., 2016):

$$\tau_c = C\rho_w\overline{w_t^2} \tag{5}$$

In which ρ_w is seawater density, constant coefficient C=0.9, and $\overline{w_t^2}$ is the change rate of near-bed vertical turbulent velocity.

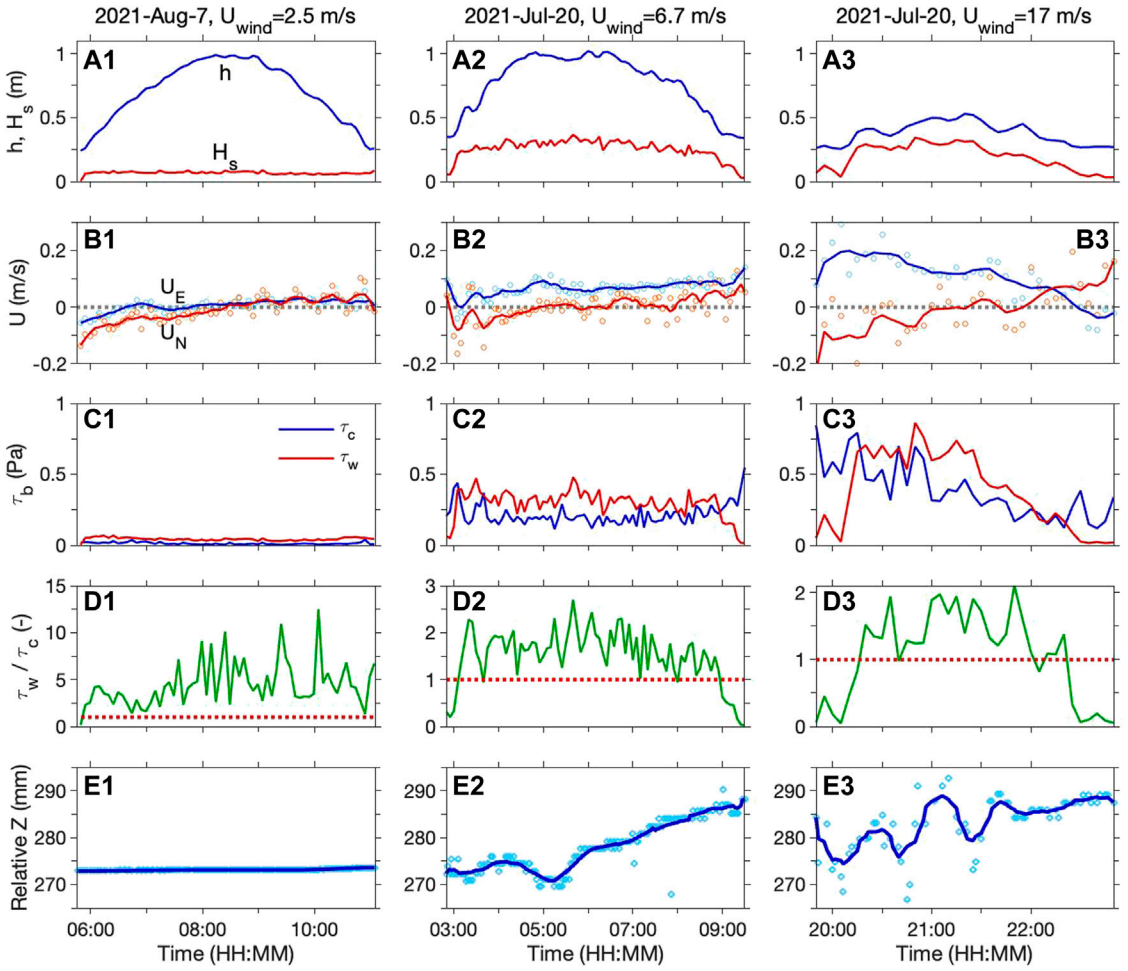

FIGURE 5
Time series of **(A)** water level (h), significant wave height (H_s), **(B)** eastward (U_E) and northward (U_N) current velocities, **(C)** current- and wave-induced bed shear stress (τ_c and τ_w), **(D)** ratio of τ_w and τ_c, and **(E)** relative bed level (Z) changes during Period 2.

Results

Tides, wind and waves

Each measurement period lasted for 1 month or 62 tidal cycles. However, because the ADV on the middle flat was equipped with probes at 0.3 or 0.5 m above the seabed, low tides were not measured. During some periods after April 18, the velocity and wave data were missed due to battery failure (Figure 2). Overall, data from 40 tidal cycles were obtained in Period 1, and data from 45 tidal cycles were obtained in Period 2.

The average wind speed during both periods was 3.0 m/s. We defined the tidal cycle during a wind event as one where the intratidal maximum wind speed exceeded 6.0 m/s. An obvious wind event occurred during each period: around April 9 during Period 1 (Figure 2A) and around July 20 during Period 2 (Figure 3A). The maximum wind speeds and predominant directions were 8.0 m/s and north-east-north in Period 1, and 17.0 m/s and north and east in Period 2, respectively (Table 1).

Measured maximum water depth, h, varied from 0.5 m to 1.7 m during Period 1 (Figure 2A), and from 0.5 m to 2.0 m during Period 2 (Figure 3B). Tides in Period 1 were irregular, i.e., the neap-spring tidal cycle was not 15 days. Significant wave height, H_s, was ordered by centimeters with mean values of 0.08 m and 0.06 m in each measurement period. The mean H_s during wind events was 2.6 times the value during calm conditions (Table 1). Correspondingly, the wave-induced bed shear stress, τ_w, was approximately three times larger during wind events than during calm conditions (Table 1).

The current velocity, U, showed the tide-driven spring-neap cyclicity. However, during the wind event in Period 2, U was

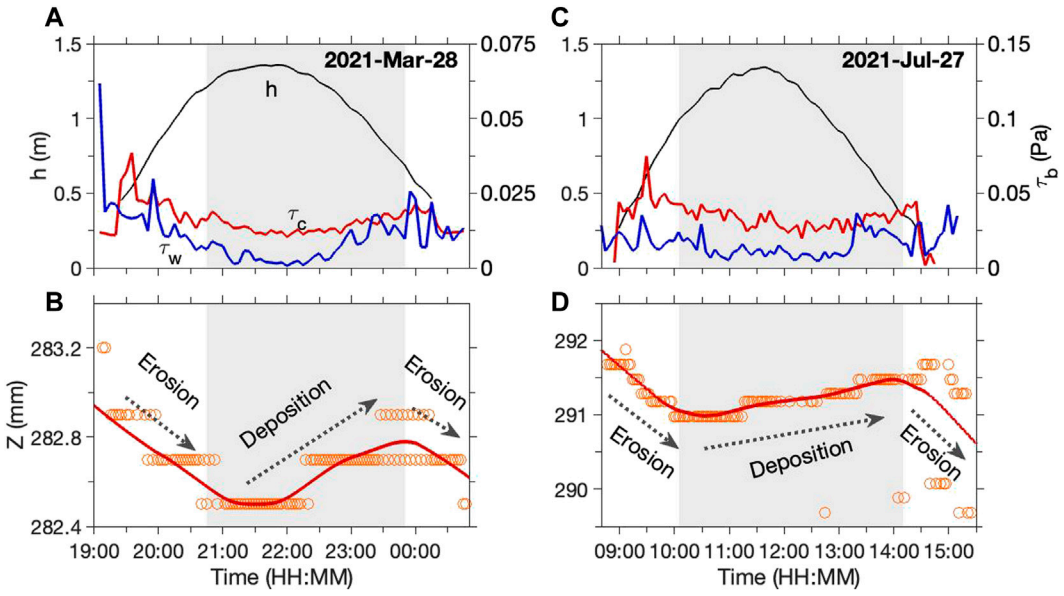

FIGURE 6
Time series of water depth (h), wave-induced bed shear stress (τ_w), current-induced bed shear stress (τ_c), relative bed level (Z, orange circle) and smoothed bed level (red line) of the calm tidal cycles. Bed erosion occurs in flood and ebb peaks, while deposition during slack water.

greater than normal values (Figure 5E). Thus, the current-induced bed shear stress, τ_c, was four times larger during wind events than during calm conditions.

Bed level changes

The bed level, Z, was relative stable without obvious spring-neap tidal cyclicity (Figure 3G and Figure 5G). The bed level statistics showed that the standard deviation was 3.0 mm. This indicates that the inter-tidal bed level change was generally at the millimeter level. During wind events, the bed level variation reached 26–27 mm.

During a typical calm tidal cycle, the bed level remained nearly constant (Figure 4D1 and Figure 5D1). Several tidal cycles show erosion-deposition-erosion cyclicity corresponding to the peak-slack-peak process (Figure 6). In contrast, the intratidal bed levels during wind events showed different patterns. During the wind events of Period 1, there were three patterns of bed-level changes:

(1) Type I: cyclicity motion (Figure 4D2 and Figure 5D3): the April 9 tidal cycle showed clear cyclicity in a period of approximately 2 h. The impact of waves (τ_w) was stronger than that of currents (τ_c) in this case.
(2) Type II: intratidal variation without clear cyclicity motion (Figure 4E3 and Figure 5E2). When both current and wave were strong, the time series of the bed-level change was more complex. There was no standard variation pattern as the bed dynamics are controlled by both hydrodynamics and sediment supply.

The maximum variation in the bed level during each tidal cycle, ΔZ, was used to quantify the intratidal bed-level dynamics. ΔZ was less than 10 mm for 90% of the measurement period and during relatively calm conditions (wind speed <6.0 m/s) (Figure 7A). As the wind speed increased, ΔZ increased correspondingly. The linear regression analysis showed that ΔZ has a stronger relationship with bottom orbital velocity (U_δ) and τ_w than current velocity (U) and τ_c (Figure 6). This indicates that bed-level changes are more sensitive to waves.

Discussion

Difference between sheltered and open mudflats

Mudflat bed is composed of fine sediments, which are sensitive to hydrodynamic disturbances. Sheltered mudflats are less dynamic than open mudflats (Hu et al., 2017). For instance, monthly variations in the bed levels of open mudflats in the meso-to macro-tidal range reached 10–30 cm (Miao et al., 2016; Zhu et al., 2017). Even the bed variation can be measured in centimeters under normal weather conditions (Zhu

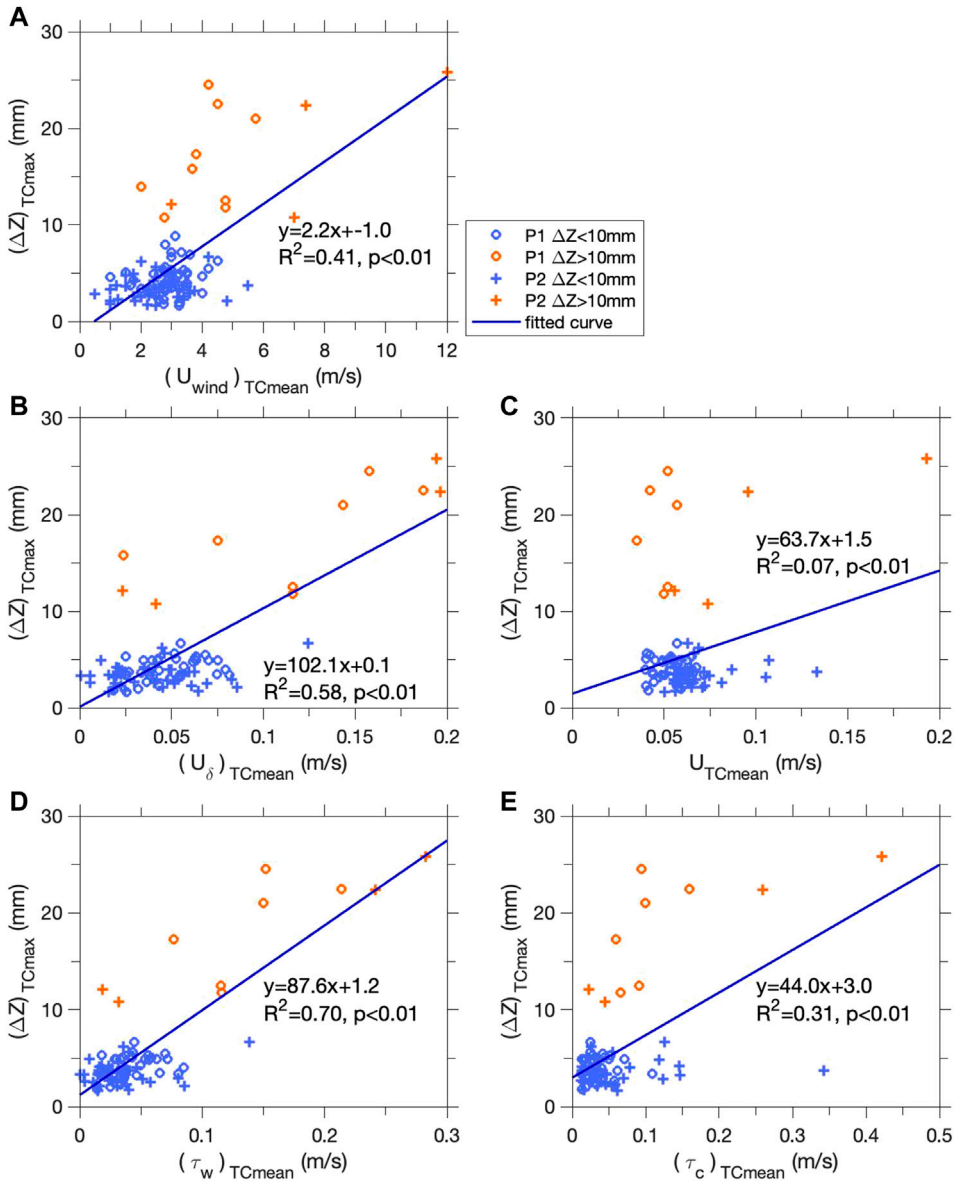

FIGURE 7
Relationship between the maximum intratidal bed-level variation, ΔZ, and **(A)** mean wind speed during each tidal cycle $(U_{wind})_{TCmean}$, **(B)** tidal-averaged bottom orbital velocity, $(U_{\delta})_{TCmean}$, **(C)** tidal-averaged current velocity, U_{TCmean}, **(D)** tidal-averaged wave-induced bed shear stress, $(\tau_w)_{TCmean}$, and **(E)** tidal-averaged current-induced bed shear stress $(\tau_c)_{TCmean}$.

et al., 2014). In brief, if a mudflat is open and exposed to strong hydrodynamic forcing, daily and monthly bed variations are in the order of centimeters and tens of centimeters, respectively. In contrast, sheltered mudflats were quite stable. Our study shows that the monthly bed variation was only approximately 1 cm. These sheltered mudflats can sometimes be stable over a longer time scale. Studies of sheltered mudflats in the Western Scheldt Estuary, the Netherlands, showed that the bathymetry profile was stable, with the variation of bed level less than 10 cm over a period of 25 years (de Vet et al., 2017; Maan et al., 2018). A stable bed environment is a potentially advantageous for maintaining the biodiversity and biomass of wetland plants and benthic animals on sheltered mudflats (Herman et al., 2001; Chargulaf and Tibbetts, 2015).

Bed-level changes between tidal submergence, which are measured by the double/triple-rod method, buried-plate measurements or optical detections, are useful for understanding the daily evolution of mudflats (Yang et al., 2003; Hu et al., 2015; Zhu et al., 2017). However, acoustic ranging detection shows that the maximum intratidal bed

level variation is much greater than the net intertidal bed level changes. This phenomenon is notable in open mudflat systems (Zhu et al., 2014; Zhu et al., 2017). The tidal cycle on the morning of April 9 demonstrates the same phenomenon on sheltered flat. The intratidal maximum variation was 20 mm, whereas the net intertidal bed-level change was 9 mm (Figure 7E2). To date, the acoustic measurement of bed surface dynamics at high temporal resolution is the only approach for determining intratidal bed level changes (Thorne et al., 2018; Zhu et al., 2019). By applying advanced acoustic bed detection, our study further indicates that the sheltered mudflat is more variable as we expected.

Intratidal bed level changes of sheltered mudflat

The typical intratidal bed-level changes in normal weather are shown in Figure 6E1 and Figure 7E1. There may be a slight trend, and the bed level was nearly constant in general. This agrees with the measurements from other sheltered mudflats (Zhu et al., 2019). Some tidal cycle still shows the cyclicity of erosion during flood and peak and deposition during slack water (Figure 6). Notably, the minimum ΔZ was larger than 1 mm, which is the accuracy of bed level detection. So far, the accuracy of acoustic bed detection is ± 1–2 mm, depending on individual instrument (Gallagher et al., 1996; Thornton et al., 1998; Christie et al., 1999; Andersen et al., 2006; Turner et al., 2008). In calm weather, both wave-and current-induced bed shear stresses were less than 0.1 Pa (Figure 6C1 and Figure 7C1), which is the typical value of critical bed shear stress for mud erosion (Winterwerp et al., 2012). No erosion and little deposition lead to a stable bed level with a slight accumulation of sediment. In our study, 73.7% of the measured ΔZ was <5 mm, indicating the stability of the sheltered mudflat. When the tidal-averaged wind speed was >3.0 m/s, more drastic intratidal bed-level changes were observed. The mechanism of local bed-level change differed from that of hydrodynamic conditions.

The observed fluctuation in the bed level was partially caused by measurement errors and accuracy issues, as mentioned above. By incorporating a moving average and despike, such noise signals can be minimized. The smoothed bed-level series exhibited a periodic signal (Figure 4D2). We defined this as the Type I bed-level variation pattern, which was closely related to the formation and migration of bed ripples. The magnitude and period of the bed-level fluctuation, referring to ripple height and ripple migration periods, were 1–2 cm and 1–2 h, respectively. This matches the typical ripple migration parameters of mudflats (Baas et al., 2013; Lin and Venditti, 2013; Zhu, 2017). Under dynamic environments with changing currents and waves, reworking and mobilization of bed sediments leads to formation of bed ripples in coastal systems (Catano-Lopera and Garcia, 2006; Thorne et al., 2018; Guerrero and Guillen, 2020; Guerrero et al., 2021; Stella, 2021). Bed ripples preferably occur in the presence of waves (Chakraborty, 2001; Lorenz and Valdez, 2011; Guerrero and Guillen, 2020; Jin et al., 2020). For the tidal cycle on the morning of April 9, τ_c was as low as 0.1 Pa due to low tide, meaning that flow could hardly stir up surface bed sediment, whereas τ_w was 2.5 times higher (Figure 4D2). Such wave-dominated conditions further prove that the Type I bed-level variation is caused by ripple migration.

Type II intratidal bed-level variations show an unclear fluctuation pattern. A typical example is the tidal cycle observed on July 20 morning (Figure 5E2). Both τ_c and τ_w were greater than 0.1 Pa, and they are comparable. This means that both the current and waves played a role in bed sediment movement. Under normal weather conditions, the intratidal bed level shows a pattern of degradation during tidal flood and ebb peaks, and accretion during high slack water on open flats (Andersen et al., 2007; Zhu et al., 2014). However, a continuous accretion trend was observed in the tidal cycle of July 20. During wind events, wind-induced flow (Figure 3D) and wind-induced turbulence result in that τ_c does not increase with tides (Figures 3, 4F) (Banerjee et al., 2015; Su et al., 2015). Meanwhile, the advection of sediment flow was strong during wind events. These two factors may break the peak-slack water cyclicity, but accretion or degradation trends are determined by the timing of wind event with regard to tidal cycle, sediment supply, residual flow, and settling time (Ding et al., 2003; Freeman et al., 2015; Xu et al., 2015; Zhu et al., 2017). The bed-level change pattern of the middle tidal flat was the most dynamic and difficult to predict (Fan et al., 2006). Additionally, there was no clear ripple migration signal in the bed-level series, as sheet flow during wind events tends to wash out ripples (Li and Amos, 1999; Thorne et al., 2018; Guerrero et al., 2021).

However, the low tide tidal cycle on July 20 (Figure 5D3) showed a different bed level pattern than that of April 9 (Figure 4D2). This cycle marked the transition between Type I and Type II variation, that is, the intratidal bed level change consisted of a cyclic motion and continuous accretion trend. The tidal conditions of the two tidal cycles were similar, but the current flow was quite different. Wind direction was offshore during Period 1 and almost onshore during Period 2 (Figure 2A and Figure 3A). Correspondingly, tidal flow was less influenced by winds during Period 1 (Figure 4B2), or by the northern component of the flow velocity (Figure 5B3). However, the eastern component was considerably influenced (Figure 5B3). There was an eastward flow during the majority of the tidal cycle, which was likely driven by wind induced flow pattern. Both τ_c and τ_w were much higher than those of other tidal cycles, reaching up to 0.7 Pa.

In summary, wave and tide conditions determine the intratidal bed level changes: 1) low τ_c and low τ_w lead to a stable bed; 2) low τ_c and high τ_w promote the generation and migration of bed ripples (Type I); 3) comparable τ_c and τ_w, with medium-to-high values lead to non-cyclicity bed-level change

patterns (Type II); and 4) high τ_c and high τ_w result in a combination of Type I and Type II variations.

Sensitivity of sheltered mudflat and its implications

Sheltered mudflats is considered stable, with the bed-level-change is in the order of millimeters in the time scale of tidal-cycle to even month, and is less affected by winds (Andersen et al., 2006; Hu et al., 2017). However, sheltered mudflats may be more dynamic than previously believed. Our study shows that the critical wind speed triggering distinct changes in the local sediment bed is approximately 3.0 m/s, a light-to-gentle breeze according to the Beaufort wind scale. If the wind is onshore, the bed-level-change can immediately respond to the wind. Otherwise, the bed need about one tidal cycle, i.e., half a day, to respond to wind. Therefore, more significant morphological changes would be expected during gale or storm events, wherein wind speed exceeds 15 m/s.

Although the sheltered mudflat is easily disturbed, it also recovers rapidly. The monthly bed-level measurements showed that the bed level fluctuated at a nearly constant level (Figures 2, 3G). These sheltered mudflats are stable and can recover quickly even after disturbance (Maan et al., 2018). For tidal flats, rapid recovery of disturbed sediment beds is enabled by the redistribution of sediments from high-energy to low-energy areas (Yang et al., 2003; Friedrichs, 2011). For low dynamic tidal flats, such as a sheltered flat, the distance of sediment movement may be smaller than in open tidal flats, and are likely to be transported back to maintain an equilibrium state after wind events (Zhu et al., 2017). The sediment transport patterns of sheltered mudflat systems must be further studied on a horizontal spatial scale.

Conclusion

In situ bed-level and hydrodynamic measurements on a sheltered mudflat were conducted in 1 month during each of the two seasons. The bed level was stable during calm weather during which wave and current forcing (τ_w and τ_c) are low. However, the sheltered mudflat was more variable than previously thought. The threshold wind speed to promote obvious intratidal bed-level variation patterns is 3.0 m/s, which generates wave heights of approximately 0.1 m. The intratidal bed-level variation patterns depend on hydrodynamic conditions: low τ_c and high τ_w promote the generation and migration of bed ripples (Type I); comparable τ_c and τ_w, with medium-to-high values, lead to non-cyclicity bed-level change patterns (Type II); and high τ_c and high τ_w result in bed accumulation/degradation superimposed by bed ripple migration, which is a combination of Type I and Type II variations. From a long-term perspective, i.e. in the time scale of month to year, sheltered mudflats are stable systems, and their high sensitivity causes short-term drastic bed-level variation, which may be harmful to benthos. The sensitivity and stability of sheltered mudflats must be further investigated under global climate change conditions.

Data availability statement

The raw data supporting the conclusions of this article will be made available by the authors, without undue reservation.

Author contributions

QZ, WN and ZZ conducted the field experiments. QZ, WN conceived the idea, carried out data analysis and draft the manuscript, YC and ZY reviewed and edited the manuscript.

Funding

This study was supported by Southern Marine Science and Engineering Guangdong Laboratory (Guanghzou) (GML202209), the Program for Guangdong Introducing Innovative and Entrepreneurial Teams (2019ZT08L213), and National Natural Science Foundation of China (51909038; 41901126).

Conflict of interest

The authors declare that the research was conducted in the absence of any commercial or financial relationships that could be construed as a potential conflict of interest.

Publisher's note

References

Andersen, T. J., Fredsoe, J., and Pejrup, M. (2007). *In situ* estimation of erosion and deposition thresholds by Acoustic Doppler Velocimeter (ADV). *Estuar. Coast. Shelf Sci.* 75, 327–336. doi:10.1016/j.ecss.2007.04.039

Andersen, T. J., Pejrup, M., and Nielsen, A. A. (2006). Long-term and high-resolution measurements of bed level changes in a temperate, microtidal coastal lagoon. *Mar. Geol.* 226, 115–125. doi:10.1016/j.margeo.2005.09.016

Baas, J. H., Davies, A. G., and Malarkey, J. (2013). Bedform development in mixed sand-mud: The contrasting role of cohesive forces in flow and bed. *Geomorphology* 182, 19–32. doi:10.1016/j.geomorph.2012.10.025

Banerjee, T., Muste, M., and Katul, G. (2015). Flume experiments on wind induced flow in static water bodies in the presence of protruding vegetation. *Adv. Water Resour.* 76, 11–28. doi:10.1016/j.advwatres.2014.11.010

Bassoullet, P., Le Hir, P., Gouleau, D., and Robert, S. (2000). Sediment transport over an intertidal mudflat: Field investigations and estimation of fluxes within the "baie de Marenngres-oleron" (France). *Cont. Shelf Res.* 20, 1635–1653. doi:10.1016/s0278-4343(00)00041-8

Blum, M. D., and Roberts, H. H. (2009). Drowning of the Mississippi Delta due to insufficient sediment supply and global sea-level rise. *Nat. Geosci.* 2, 488–491. doi:10.1038/ngeo553

Catano-Lopera, Y. A., and Garcia, M. H. (2006). Geometry and migration characteristics of bedforms under waves and currents - Part 2: Ripples superimposed on sandwaves. *Coast. Eng.* 53, 781–792. doi:10.1016/j.coastaleng.2006.03.008

Callaghan, D. P., Bouma, T. J., Klaassen, P., Van Der Wal, D., Stive, M. J. F., and Herman, P. M. J. (2010). Hydrodynamic forcing on salt-marsh development: Distinguishing the relative importance of waves and tidal flows. *Estuar. Coast. Shelf Sci.* 89, 73–88. doi:10.1016/j.ecss.2010.05.013

Chakraborty, C. (2001). Lagoon-tidal flat sedimentation in an epeiric sea: Proterozoic bhander group, son valley, India. *Geol. J.* 36, 125–141. doi:10.1002/gj.884

Chargulaf, C. A., and Tibbetts, I. R. (2015). Spatial and temporal variation of meiofauna community structure in soft-sediment pools around Moreton Bay, Australia. *Aust. J. Zool.* 63, 204–213. doi:10.1071/zo14063

Christie, M. C., Dyer, K. R., and Turner, P. (1999). Sediment flux and bed level measurements from a macro tidal mudflat. *Estuar. Coast. Shelf Sci.* 49, 667–688. doi:10.1006/ecss.1999.0525

Costanza, R., Darge, R., Degroot, R., Farber, S., Grasso, M., Hannon, B., et al. (1997). The value of the world's ecosystem services and natural capital. *Nature* 387, 253–260. doi:10.1038/387253a0

De Vet, P. L. M., Van Prooijen, B. C., and Wang, Z. B. (2017). The differences in morphological development between the intertidal flats of the Eastern and Western Scheldt. *Geomorphology* 281, 31–42. doi:10.1016/j.geomorph.2016.12.031

Ding, P., Hu, K., Kong, Y., and Hu, D. (2003). Numerical simulation of storm-induced erosion/deposition in yangtze estuary --A case study of typhoon jelawat. *J. Sediment Res.* 0, 18–24.

Fan, D. D., Guo, Y. X., Wang, P., and Shi, J. Z. (2006). Cross-shore variations in morphodynamic processes of an open-coast mudflat in the Changjiang Delta, China: With an emphasis on storm impacts. *Cont. Shelf Res.* 26, 517–538. doi:10.1016/j.csr.2005.12.011

Freeman, A. M., Jose, F., Roberts, H. H., and Stone, G. W. (2015). Storm induced hydrodynamics and sediment transport in a coastal Louisiana lake. *Estuar. Coast. Shelf Sci.* 161, 65–75. doi:10.1016/j.ecss.2015.04.011

Friedrichs, C. T. (2011). "Tidal flat morphodynamics: A synthesis," in *Treatise on estuarine and coastal science*. Editors J. D. Hansom and B. W. Flemming (Amsterdam, Netherlands: Elsevier).

Gallagher, E. L., Boyd, W., Elgar, S., Guza, R. T., and Woodward, B. (1996). Performance of a sonar altimeter in the nearshore. *Mar. Geol.* 133, 241–248. doi:10.1016/0025-3227(96)00018-7

Goodwin, I. D., Mortlock, T. R., and Browning, S. (2016). Tropical and extratropical-origin storm wave types and their influence on the East Australian longshore sand transport system under a changing climate. *J. Geophys. Res. Oceans* 121, 4833–4853. doi:10.1002/2016jc011769

Grant, W. D., and Madsen, O. S. (1979). Combined wave and current interaction with a rough bottom. *J. Geophys. Res.* 84, 1797–1808. doi:10.1029/jc084ic04p01797

Guerrero, Q., and Guillen, J. (2020). Dynamics of ripples superimposed on a sand ridge on a tideless shoreface. *Estuar. Coast. Shelf Sci.* 242, 106826. doi:10.1016/j.ecss.2020.106826

Guerrero, Q., Williams, M. E., Guillén, J., Lichtman, I. D., Thorne, P. D., and Amoudry, L. O. (2021). Small-scale bedforms and associated sediment transport in a macro-tidal lower shoreface. *Cont. Shelf Res.* 225, 104483. doi:10.1016/j.csr.2021.104483

Herman, P. M. J., Middelburg, J. J., and Heip, C. H. R. (2001). Benthic community structure and sediment processes on an intertidal flat: Results from the ECOFLAT project. *Cont. Shelf Res.* 21, 2055–2071. doi:10.1016/s0278-4343(01)00042-5

Hu, Z., Wang, Z. B., Zitman, T. J., Stive, M. J. F., and Bouma, T. J. (2015). Predicting long-term and short-term tidal flat morphodynamics using a dynamic equilibrium theory. *J. Geophys. Res. Earth Surf.* 120, 1803–1823. doi:10.1002/2015jf003486

Hu, Z., Yao, P., Van Der Wal, D., and Bouma, T. J. (2017). Patterns and drivers of daily bed-level dynamics on two tidal flats with contrasting wave exposure. *Sci. Rep.* 7, 7088. doi:10.1038/s41598-017-07515-y

Hu, Z., Zhou, J., Wang, C., Wang, H., He, Z., Peng, Y., et al. (2020). A novel instrument for bed dynamics observation supports machine learning applications in mangrove biogeomorphic processes. *Water Resour. Res.* 56. doi:10.1029/2020wr027257

Jestin, H., Bassoullet, P., Le Hir, P., L'yavanc, J., and Degres, Y. (1998). "Development of ALTUS, a high frequency acoustic submersible recording altimeter to accurately monitor bed elevation and quantify deposition and erosion of sediments," in IEEE Oceanic Engineering Society. OCEANS'98. Conference Proceedings, Nice, France, 28 September 1998 - 01 October 1998. 98, 189-194.

Jin, C., Coco, G., Tinoco, R. O., Perron, J. T., Myrow, P. M., Huppert, K. L., et al. (2020). Investigating the response of wave-generated ripples to changes in wave forcing. *Geomorphology* 363, 107229. doi:10.1016/j.geomorph.2020.107229

Kim, S. C., Friedrichs, C. T., Maa, J. P. Y., and Wright, L. D. (2000). Estimating bottom stress in tidal boundary layer from Acoustic Doppler Velocimeter data. *J. Hydraul. Eng.* 126, 399–406. doi:10.1061/(asce)0733-9429(2000)126:6(399)

Klein, A. H. D., and De Menezes, J. T. (2001). Beach morphodynamics and profile sequence for a headland bay coast. *J. Coast. Res.* 17, 812–835.

Lorenz, R. D., and Valdez, A. (2011). Variable wind ripple migration at great sand dunes national park and preserve, observed by timelapse imaging. *Geomorphology* 133, 1–10. doi:10.1016/j.geomorph.2011.06.003

Li, C., Wang, P., Daidu, F., Bing, D., and Tiesong, L. (2000). Open-coast intertidal deposits and the preservation potential of individual laminae: A case study from east-central China. *Wiley* 47, 1051. doi:10.1046/j.1365-3091.2000.00338.x

Li, M. Z., and Amos, C. L. (1999). Sheet flow and large wave ripples under combined waves and currents: Field observations, model predictions and effects on boundary layer dynamics. *Cont. Shelf Res.* 19, 637–663. doi:10.1016/s0278-4343(98)00094-6

Lin, C. Y. M., and Venditti, J. G. (2013). An empirical model of subcritical bedform migration. *Sedimentology* 60, 1786–1799. doi:10.1111/sed.12056

Liu, S., Li, X., Chen, D., Duan, Y., and Zhang, L. (2020). Understanding Land use/Land cover dynamics and impacts of human activities in the Mekong Delta over the last 40 years. *Glob. Ecol. Conservation* 22, e00991. doi:10.1016/j.gecco.2020.e00991

Maan, D. C., Van prooijen, B. C., Zhu, Q., and Wang, Z. B. (2018). Morphodynamic feedback loops control stable fringing flats. *J. Geophys. Res. Earth Surf.* 0, 2993–3012. doi:10.1029/2018jf004659

Macmahan, J., Brown, J., Brown, J., Thornton, E., Reniers, A., Stanton, T., et al. (2010). Mean Lagrangian flow behavior on an open coast rip-channeled beach: A new perspective. *Mar. Geol.* 268, 1–15. doi:10.1016/j.margeo.2009.09.011

Madsen, A. T., Murray, A. S., Andersen, T. J., and Pejrup, M. (2010). Spatial and temporal variability of sediment accumulation rates on two tidal flats in Lister Dyb tidal basin, Wadden Sea, Denmark. *Earth Surf. Process. Landf.* 35, 1556–1572. doi:10.1002/esp.1999

Mclachlan, R. L., Ogston, A. S., Asp, N. E., Fricke, A. T., Nittrouer, C. A., and Schettini, C. a. F. (2020). Morphological evolution of a macrotidal back-barrier environment: The Amazon Coast. *Sedimentology* 67, 3492–3512. doi:10.1111/sed.12752

Miao, L. M., Yang, S. L., Zhu, Q., Shi, B. W., Li, P., and Wu, C. S. (2016). Variations of suspended sediment concentration and transport in response to a storm and its dynamic mechanism - a study case of Nanhui tidal flat of the Yangtze River Delta. *Acta Oceanol. Sin.* 38, 158–167.

Milliman, J. D., and Farnsworth, K. L. (2011). River Discharge to the coastal ocean – a global synthesis. *River discharge to the coastal ocean – a global synthesis*. Cambridge: Cambridge University Press.

Nansingh, P., and Jurawan, S. (1999). Environmental sensitivity of a tropical coastline (Trinidad, West Indies) to oil spills. *Spill Sci. Technol. Bull.* 5, 161–172. doi:10.1016/s1353-2561(98)00052-8

Nicholls, R. J., Hoozemans, F., and Marchand, M. (1999). Increasing flood risk and wetland losses due to global sea-level rise: Regional and global analyses. *Glob. Environ. Change* 9, S69–S87. doi:10.1016/s0959-3780(99)00019-9

Nortek, A. S. (2005). Vector current meter user manual, Norway, 15.

Paavo, B. L., Ham, D., Goerlitz, S., and Probert, P. K. (2012). How does tidal submersion time affect macroinvertebrate community patterns on a temperate sheltered sandflat? *Mar. Freshw. Res.* 63, 68–77. doi:10.1071/mf11147

Reckhardt, A., Beck, M., Seidel, M., Riedel, T., Wehrmann, A., Bartholomae, A., et al. (2015). Carbon, nutrient and trace metal cycling in sandy sediments: A comparison of high-energy beaches and backbarrier tidal flats. *Estuar. Coast. Shelf Sci.* 159, 1–14. doi:10.1016/j.ecss.2015.03.025

Ryu, S. O. (2003). Seasonal variation of sedimentary processes in a semi-enclosed bay: Hampyong bay, Korea. *Estuar. Coast. Shelf Sci.* 56, 481–492. doi:10.1016/s0272-7714(02)00199-3

Saulter, A. N., Russell, P. E., Gallagher, E. L., and Miles, J. R. (2003). Observations of bed level change in a saturated surf zone. *J. Geophys. Res.* 108, 3112. doi:10.1029/2000jc000684

Schuerch, M., Spencer, T., Temmerman, S., Kirwan, M. L., Brown, S., Lincke, D., et al. (2018). Future response of global coastal wetlands to sea-level rise. *Nature* 561, 231–234. doi:10.1038/s41586-018-0476-5

Shen, Y., Jia, H., Li, C., and Tang, J. (2018). Numerical simulation of saltwater intrusion and storm surge effects of reclamation in Pearl River Estuary, China. *Appl. Ocean Res.* 79, 101–112. doi:10.1016/j.apor.2018.07.013

Siegle, E., Dottori, M., and Villamarin, B. C. (2018). Hydrodynamics of a subtropical tidal flat: Araca Bay, Brazil. *Ocean Coast. Manag.* 164, 4–13. doi:10.1016/j.ocecoaman.2017.11.003

Stella, M. (2021). Morphodynamics of the south Baltic seabed in the remote nearshore zone in the light of field measurements. *Mar. Geol.* 439, 106546. doi:10.1016/j.margeo.2021.106546

Su, M., Yao, P., Wang, Z. B., Chen, Y. P., Zhang, C. K., and Stive, M. J. F. (2015). "Laboratory studies on the response of fine sediment to wind," in *IAHR world congress 2015* (Netherlands: the Netherlands: IHAR).

Temmerman, S., Meire, P., Bouma, T. J., Herman, P. M. J., Ysebaert, T., and De Vriend, H. J. (2013). Ecosystem-based coastal defence in the face of global change. *Nature* 504, 79–83. doi:10.1038/nature12859

Thorne, P. D., Hurther, D., Cooke, R. D., Caceres, I., Barraud, P. A., and Sanchez-Arcilla, A. (2018). Developments in acoustics for studying wave-driven boundary layer flow and sediment dynamics over rippled sand-beds. *Cont. Shelf Res.* 166, 119–137. doi:10.1016/j.csr.2018.07.008

Thornton, E. B., Swayne, J. L., and Dingler, J. R. (1998). Small-scale morphology across the surf zone. *Mar. Geol.* 145, 173–196. doi:10.1016/s0025-3227(97)00114-x

Tucker, M. J., and Pitt, E. G. (2001). *Waves in ocean engineering*. Amsterdam, Netherlands: Elsevier.

Turner, I. L., Russell, P. E., and Butt, T. (2008). Measurement of wave-by-wave bed-levels in the swash zone. *Coast. Eng.* 55, 1237–1242. doi:10.1016/j.coastaleng.2008.09.009

Vafeidis, A. T., Nicholls, R. J., Mcfadden, L., Tol, R., Hinkel, J., Spencer, T., et al. (2008). A new global coastal database for impact and vulnerability analysis to sea-level rise. *J. Coast. Res.* 24, 917–924. doi:10.2112/06-0725.1

Van Rijn, L. C. (1993). *Principles of sediment transport in rivers, estuaries and coastal seas*. Amsterdam, Netherlands: Aqua Publication.

Walling, D. E. (2006). Human impact on land–ocean sediment transfer by the world's rivers. *Geomorphology* 79, 192–216. doi:10.1016/j.geomorph.2006.06.019

Wang, Z., Van Maren, D., Ding, P., Yang, S., Van Prooijen, B., De Vet, P., et al. (2015). Human impacts on morphodynamic thresholds in estuarine systems. *Cont. Shelf Res.* 111, 174–183. doi:10.1016/j.csr.2015.08.009

Waska, H., and Kim, G. (2010). Differences in microphytobenthos and macrofaunal abundances associated with groundwater discharge in the intertidal zone. *Mar. Ecol. Prog. Ser.* 407, 159–172. doi:10.3354/meps08568

Williams, J. J., Bell, P. S., and Thorne, P. D. (2003). Field measurements of flow fields and sediment transport above mobile bed forms. *J. Geophys. Res.* 108, 3109. doi:10.1029/2002jc001336

Winterwerp, J. C., Van Kesteren, W. G. M., Van Prooijen, B., and Jacobs, W. (2012). A conceptual framework for shear flow-induced erosion of soft cohesive sediment beds. *J. Geophys. Res.* 117, 17. doi:10.1029/2012jc008072

Xu, K., Mickey, R. C., Chen, Q., Harris, C. K., Hetland, R. D., Hu, K., et al. (2015). Shelf sediment transport during hurricanes Katrina and Rita. *Comput. Geosciences* 8, 24–39. doi:10.1016/j.cageo.2015.10.009

Yang, B. C., Dalrymple, R. W., and Chun, S. S. (2005). Sedimentation on a wave-dominated, open-coast tidal flat, south-Western Korea: Summer tidal flat-winter shoreface. *Sedimentology* 52, 235–252. doi:10.1111/j.1365-3091.2004.00692.x

Yang, S. L., Friedrichs, C. T., Shi, Z., Ding, P. X., Zhu, J., and Zhao, Q. Y. (2003). Morphological response of tidal marshes, flats and channels of the outer Yangtze River mouth to a major storm. *Estuaries* 26, 1416–1425. doi:10.1007/bf02803650

Yang, S. L., Milliman, J. D., Li, P., and Xu, K. (2011). 50, 000 dams later: Erosion of the Yangtze River and its delta. *Glob. Planet. Change* 75, 14–20. doi:10.1016/j.gloplacha.2010.09.006

Zhu, Q. (2017). *Sediment dynamics on intertidal mudflat: A study based on* in situ *measurements and numerical modelling*. Netherland: Delft University of Technology.

Zhu, Q., Van Prooijen, B., Wang, Z., and Yang, S. (2017). Bed-level changes on intertidal wetland in response to waves and tides: A case study from the yangtze river delta. *Mar. Geol.* 385, 160–172. doi:10.1016/j.margeo.2017.01.003

Zhu, Q., Van Prooijen, B. C., Maan, D. C., Wang, Z. B., Yao, P., Daggers, T., et al. (2019). The heterogeneity of mudflat erodibility. *Geomorphology* 345, 106834. doi:10.1016/j.geomorph.2019.106834

Zhu, Q., Van Prooijen, B. C., Wang, Z. B., Ma, Y. X., and Yang, S. L. (2016). Bed shear stress estimation on an open intertidal flat using *in situ* measurements. *Estuar. Coast. Shelf Sci.* 182, 190–201. doi:10.1016/j.ecss.2016.08.028

Zhu, Q., Yang, S., and Ma, Y. (2014). Intra-tidal sedimentary processes associated with combined wave–current action on an exposed, erosional mudflat, southeastern Yangtze River Delta, China. *Mar. Geol.* 347, 95–106. doi:10.1016/j.margeo.2013.11.005

Zhu, S. X., Yang, H. L., Zhu, C., Wang, P., and Ying, Q. Z. (2008). The inter-tidal macrobenthic benthic community characters of Zhapo, Guangdong. *J. Zhejiang Ocean Univ. Nat. Sci.* 27, 22–27.